

# Wave driven fast ion loss in the National Spherical Torus Experiment

E. D. Fredrickson, C. Z. Cheng, D. Darrow, G. Fu, N. N. Gorelenkov, G. Kramer,  
S. S. Medley, J. Menard, and L. Roquemore  
*Princeton Plasma Physics Laboratory, Princeton, New Jersey 08543*

D. Stutman  
*Johns Hopkins University, Baltimore, Maryland 21218*

R. B. White  
*Princeton Plasma Physics Laboratory, Princeton, New Jersey 08543*

(Received 16 January 2003; accepted 4 April 2003)

Spherical tokamaks have relatively low toroidal field which means that the fast-ion Larmor radius is relatively large ( $\rho_{fi} > 0.04 a_p$ ) and the fast ion velocity is much greater than the Alfvén speed ( $V_{fi} > 2 V_{\text{Alfvén}}$ ). This regime of large Larmor radius and low Alfvén speed is a regime in which fast ion driven instabilities are potentially virulent. It is therefore an important goal of the present proof-of-principle spherical tokamaks to evaluate the role of fast ion driven instabilities in fast ion confinement. This paper presents the first observations of fast ion losses in a spherical tokamak resulting from energetic particle driven modes. Two classes of instabilities are responsible for the losses. Multiple, simultaneously bursting modes in the toroidal Alfvén eigenmode frequency gap cause neutron drops of up to 15%. A bursting, chirping mode identified as precession and/or bounce resonance fishbone also causes significant neutron drops. Both modes are usually present when the losses are observed. © 2003 American Institute of Physics. [DOI: 10.1063/1.1579493]

## I. INTRODUCTION

Losses of fast ions due to “fishbone” modes,<sup>1–4</sup> toroidal Alfvén eigenmodes (TAE),<sup>5–25</sup> and energetic particle modes (rTAE/EPM)<sup>26–31</sup> have been seen in many conventional aspect ratio tokamaks. In these experiments the fast ion population is present for the purpose of heating the plasma, and is provided by either neutral beam injection (NBI) or ion cyclotron range of frequency (ICRF) heating. These losses are of concern in that the heating of deuterium–tritium (D–T) fusion plasmas is also expected to be primarily by fast ions in the form of the super Alfvénic fusion  $\alpha$ 's.

In recognition of their potentially deleterious effects on performance in proposed D–T fusion devices, fast ion driven instabilities have been extensively studied in conventional aspect ratio tokamaks. Any substantial loss of the fusion  $\alpha$ 's would either reduce the ignition margin, or, as importantly, cause damage to plasma facing components. Theoretical modeling of these instabilities and their impact on fast ion confinement, benchmarked against experimental observations, has suggested that the large size and high field of most envisioned conventional aspect ratio tokamak fusion reactors will minimize the impact of fast ion driven instabilities. Consistent with this picture, many of the observed fast ion instabilities in the present generation of large, high field tokamaks were relatively benign.

Spherical tokamaks (STs), including the National Spherical Torus Experiment NSTX,<sup>32</sup> are particularly susceptible to fast ion driven instabilities, due primarily to their relatively low toroidal field, but also in some instances due to the direct effect of the low aspect ratio. Indeed, a wide variety of beam driven instabilities has already been seen in NSTX, at frequencies ranging from a few kilohertz to many meg-

ahertz.<sup>33–36</sup> The Alfvénic modes are readily excited in NSTX as the neutral beam full energy ion velocity is typically two to four times the Alfvén speed and because the Larmor radius of the fast ions is large compared to the minor radius, enhancing mode–particle interactions. The situation in a ST component test facility or reactor concept<sup>37</sup> will be very similar, with the fusion  $\alpha$ 's having similar dimensionless parameters to the beam ions in NSTX.

This paper will focus on two classes of fast ion driven instabilities which have recently been discovered to cause fast ion losses in NSTX. The first of these is the toroidal Alfvén eigenmode (TAE), first seen in conventional aspect ratio tokamaks during NBI and ICRF heated plasmas.<sup>5–25</sup> This instability has been extensively studied over a wide range in parameters in conventional tokamaks and in many cases implicated in enhanced transport of fast ions. The second instability is different from, but appears related to, the fishbone instability first discovered on the Poloidal Divertor Experiment (PDX) tokamak<sup>1–4</sup> and observed since on most beam heated conventional tokamaks.<sup>38,39</sup> Fishbone-like instabilities with similar characteristics to those seen on NSTX have previously been observed on both DIII-D<sup>40,41</sup> and the Small Tight Aspect Ratio Tokamak, START.<sup>42</sup> Recently a model for the instability, based on a bounce resonance, rather than a precession resonance, has been proposed.<sup>43</sup> The goal of the paper is to present an overview of some of the initial experimental data.

In Sec. II of this paper the experimental results on TAE and fishbone induced fast ion losses will be reported. In Sec. II A examples of fast ion losses due predominantly to TAE instabilities will be shown. Section II B describes examples where losses are predominantly due to a bursting-chirping

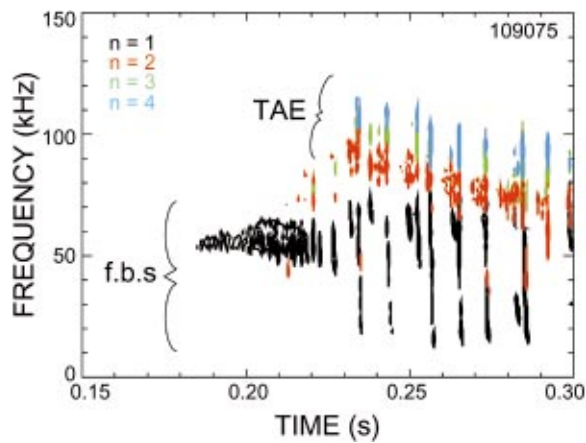


FIG. 1. (Color) Spectrogram of the signal from a Mirnov coil on NSTX during neutral beam heating showing variety of coherent modes in plasma discharge 109075. Plasma current  $\approx 700$  kA, and toroidal field 4.9 kG, and neutral beam heating power 6.1 MW at 90–95 kV. Black contours indicate  $n=1$  modes, red  $n=2$ , green  $n=3$ , and blue  $n=4$ .

mode (fishbone) and some data on the structure of the modes is presented. In Sec. II C some examples of the more common situation, where losses occur in the presence of both modes, are shown. In Sec. IV the results are discussed and areas for further experimental and theoretical work identified. The implications for future machines are briefly discussed.

The NSTX is a low aspect ratio ( $R/a \approx 1.3$ ) toroidal device. The plasma major and minor radii are 0.87 and 0.65 m, respectively. The operational parameters for beam heated plasmas are up to 1.5 MA of plasma current, 3–6 kG toroidal field at the nominal plasma major radius, central electron density is  $0.5\text{--}8 \times 10^{19}/\text{m}^3$ , central electron temperature of 0.3–1.5 keV. The plasmas were heated with 0.5–6 MW of deuterium neutral beam injection power at a voltage of up to 100 kV.

## II. EXPERIMENTAL RESULTS

An example of a typical spectrum of magnetohydrodynamic (MHD) activity during NBI heating on NSTX is shown in Fig. 1. The frequency range below 150 kHz includes the resonant toroidal Alfvén eigenmodes (rTAE) or other energetic particle modes (EPM), toroidal Alfvén eigenmodes (TAE), fishbone, and other current and pressure driven MHD modes, but excludes the “compressional” Alfvénic mode (CAE) activity.<sup>33–36,44–48</sup> The higher Alfvén gaps are also not included, but modes in the frequency range of these higher gaps have not yet been observed, consistent with theoretical predictions.<sup>49</sup> The fishbone and TAE bursts are often correlated with fast drops in the neutron rate and bursts in the D-alpha emission [Figs. 2(b) and 2(c)] on NSTX. These observations are taken to indicate losses of fast ions.

The toroidal mode numbers in the spectrogram shown in Fig. 1 and in other spectrograms are determined through phase analysis of a toroidal array of twelve Mirnov coils. The coils are mounted on the outboard vacuum vessel wall, approximately 0.48 m below the midplane. The array con-

sists of four sets of three coils each, with relative toroidal locations of  $0^\circ$ ,  $10^\circ$ , and  $30^\circ$ . The data from these coils are acquired at 500 kHz. The coil bandwidth is about 250 kHz. A subset of the coil data is acquired at 1 MHz, and higher bandwidth coils in similar locations are acquired at 5 MHz, allowing for verification that the signals are not aliased.

The low toroidal field on NSTX, as well as the relatively high rotation rates, result in a spectrum that is not as well separated as is the case in large, high field conventional aspect ratio tokamaks, where the TAE gaps are typically an order of magnitude higher in frequency than the typical MHD frequencies. On NSTX central rotation rates can be up to 20–30 kHz, while near the edge the rotation is typically 2–5 kHz. Thus, an  $n=2$  mode with zero frequency in the plasma frame can have a frequency in the lab frame from a few kilohertz to over 50 kHz. The higher end of this range, corresponding to a mode in the core, is comparable to the first, off-axis TAE gap frequencies. The initial, high frequency, phase of the fishbone instabilities, which correspond to the fast ion bounce or precession frequencies, also commonly begin near the TAE gap range of frequencies. This overlap of lab-frame frequency ranges makes identification of modes, based on frequency alone, problematic.

The TAE are a natural, weakly damped resonant oscillation of the plasma. The frequency of TAE is determined by plasma parameters such as the Alfvén velocity (a function of density and magnetic field strength) and magnetic field geometry through the TAE-gap structure. For TAE instabilities localized outside the  $q=1$  surface (to exclude fast profile changes due to sawteeth), the mode frequencies should change only slowly with time, i.e., on current diffusion or density confinement time scales. Thus modes with frequencies in the first TAE gap frequency range and whose frequency changes slowly have been tentatively identified as TAE instabilities. The TAE can have either a strongly bursting character, i.e., the mode periodically grows quickly, then disappears, or reach a quasi-saturated state where the mode amplitude evolves on equilibrium evolution time scales. This difference in behavior has been studied in the context of TAEs in conventional aspect ratio tokamaks and can be modeled by a predator–prey type relationship.<sup>16</sup> Theoretical modeling of these modes using the best available measurements of plasma equilibria have begun.<sup>49</sup>

In this same frequency range, modes which rapidly “chirp” (sweep downward) in frequency have also been seen. As changes in mode frequency on this time scale are very unlikely to represent changes in equilibrium plasma conditions, these modes are believed to be of the generic class of energetic particle modes (EPM). For these modes, the frequency is determined by the resonance condition with the fast ion distribution; the fastest mode growth rate is at the frequency that maximizes the energy transfer rate from the fast ions to the mode. As the mode grows and modifies the fast ion distribution, the mode frequency evolves to keep the drive at a maximum. The strong chirping of these particular modes on NSTX is suggestive of the fishbone instability discovered on PDX. While these modes are clearly not exactly the same, we refer to them here generically as fishbones. These modes will be discussed in more detail in Sec. II B.

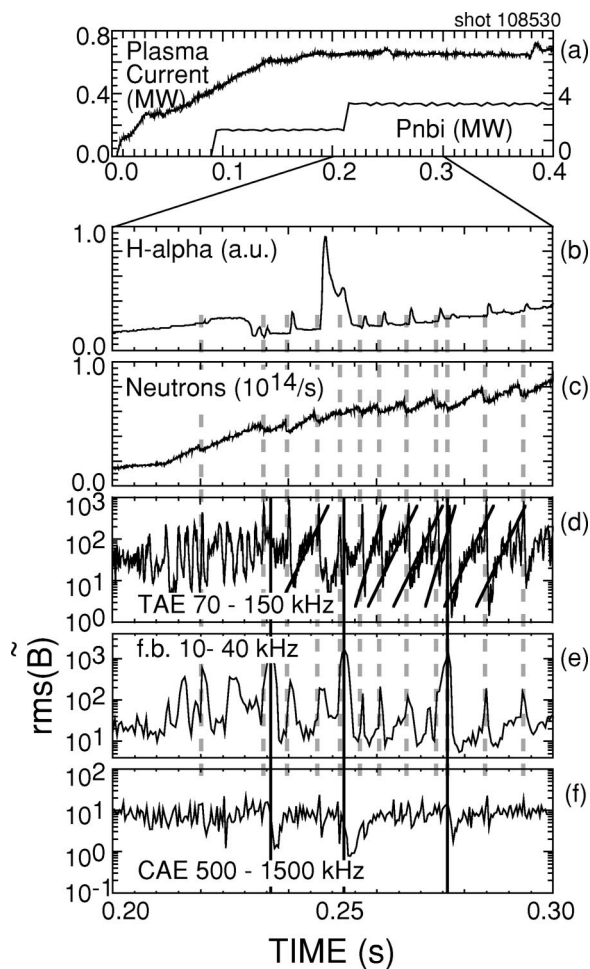


FIG. 2. Typical evolution of a NSTX discharge (toroidal field is 4.5 kG). (a) Plasma current and neutral beam heating waveform, (b) D-alpha light from the upper divertor plate, (c) volume neutron emission, (d) rms magnetic fluctuations in the 70–150 kHz band (TAE), (e) rms magnetic fluctuation level in the frequency band 10–40 kHz (fishbones), (f) rms magnetic fluctuation level in the 500–1500 kHz band (CAE modes).

### A. TAE-induced fast ion loss

For most NSTX beam heated plasmas, TAE, when present, are quasi-continuous and have no detectable effect on plasma performance. However, in experiments in which  $H$  modes, with broad density profiles, were created in plasmas with relatively high  $q$  on axis (deduced with EFIT<sup>50,51</sup>) the TAE became strongly bursting. Concurrently with the bursts, fast drops in the neutron rate were observed as well as bursts of fast-ion losses and D-alpha bursts. These observations suggest substantial losses of fast beam ions.

An example of such a shot is shown in Fig. 2. Figure 2(a) shows the time evolution of the neutral beam heating power and the plasma current for a 650 kA shot. Shortly after the beam power is stepped up to 3.2 MW, the plasma goes into  $H$  mode [evidenced by the drop in D-alpha light at 0.232 s in Fig. 2(b)]. Spikes in the D-alpha light are seen during the  $H$ -mode phase, coincident with drops in the neutron rate [Fig. 2(c)]. These spikes are not edge-localized modes (ELMs), since there is no drop in edge soft x-ray emission which occurs with ELMs. These events are correlated with strong bursts of coherent MHD activity [Fig. 2(d)]. (The neutron diagnostic timing is uncertain to  $\approx 1$  ms, precluding a

more precise correlation of the timing of the neutron drop with mode growth.)

The drop in the neutron rate is  $\approx 10\%$ – $15\%$  for each burst. The neutron production,  $S$ , is mostly from beam–target reactions ( $\approx 75\%$  beam–target,  $\approx 25\%$  beam–beam, and  $< 0.1\%$  thermal). Assuming that the lost ions are the most energetic, this drop corresponds to a similar drop in the population of the most energetic ions (the neutron production is a very steep function of the fast ion energy). The drop in fast ion density is slightly less than linear in the drop in neutron rate (because of the contribution of the beam-beam neutrons), and for small perturbations in these plasmas  $\delta n_{\text{fast}}/n_{\text{fast}} \approx 0.8 \delta S/S$ . Estimating the fast ion slowing down time to be  $\tau_{\text{slow}} \approx 55$  ms, the average period between bursts to be about  $\tau_{\text{burst}} \approx 6$  ms and the average neutron rate drop to be  $\delta S \approx 12\%$  (i.e.,  $\delta n_{\text{fast}} \approx 10\%$ ), it can be estimated that the effect, in equilibrium, of such modes would be to drop the fast ion population by approximately 50%.<sup>13,52</sup> (This assumes a constant source and the dominant fast ion energy loss mechanism, excepting the TAE bursts, to be classical slowing down.) In practice, of course, if the instabilities can cause substantial losses, they will keep the fast ion beta near the threshold for excitation.

Bursts of D-alpha light correlated with each TAE burst and neutron drop are evidence that the fast ions expelled from the plasma are striking the divertor plates. The loss of fast ions has also been independently confirmed by direct measurement of ion losses with a fast-ion loss probe.<sup>53</sup> The probe is mounted on the outboard vacuum vessel midplane. The present detectors do not resolve pitch angle or energy, but do detect bursts of loss coinciding with each TAE burst.

In Fig. 2(d) is a graph of the time evolution of the rms magnetic fluctuation level integrated over the frequency range from 80 to 150 kHz. The modes have a roughly exponential growth in the time period between the bursts. The approximate average growth rate, as indicated for a couple of bursts, is about  $500 \text{ s}^{-1}$ , or  $\gamma/\omega \approx 1.6 \times 10^{-3}$ . There is significant variation in this estimated growth rate, and the final growth rate at the end of each period does appear to be significantly larger, with  $\gamma/\omega \approx 6 \times 10^{-3}$ . The large final growth rate may be an example of the “domino” effect where many modes can be nonlinearly destabilized allowing access to more of the fast ion distribution free energy.<sup>54</sup> The peak rms TAE mode amplitude (measured at the vacuum vessel wall on the outboard midplane) has reached nearly 1 G when the neutron drop occurs.

The effect of fast ion losses on other fast ion driven modes is also of interest. The rms magnetic fluctuation levels in two other frequency bands; 10–40 kHz corresponding to the fishbone modes discussed in the following, and 500–1500 kHz corresponding to the CAE frequency band are shown in Figs. 2(e) and 2(f), respectively. Three strong fishbone bursts are seen in this time period, indicated by the bold vertical lines in the figure. Interestingly, there is no apparent effect on the TAE amplitude for the first two bursts, and none of the fishbone bursts is correlated with particularly large drops in the neutron rate. However, the drop in the CAE amplitude following each fishbone is evidence that the fishbones modify the fast ion population [Fig. 2(f)]. There is no

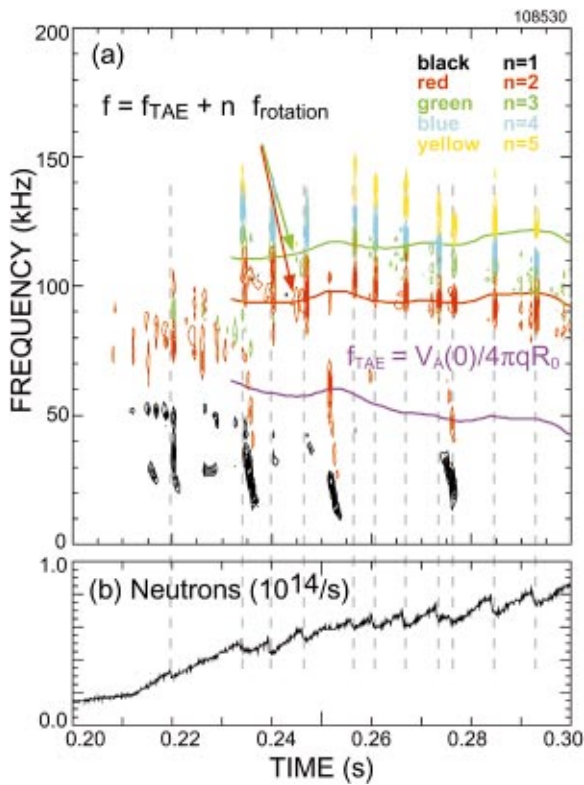


FIG. 3. (Color) Spectrogram of magnetic fluctuations showing correlation of TAE and fishbone instability bursts with neutron drops (same shot as in Fig. 2). (a) Spectrogram of a Mirnov coil signal and (b) neutron emissivity.

similar effect of the TAE bursts on the CAE, despite the drops in neutron emission correlated with the TAE bursts. These observations suggest that the TAE are excited by, and cause loss of, a different population of fast ions from those which drive the CAE, separated either in physical or phase space. The fishbones, however, interact with populations driving both CAE and TAE (the TAE bursts often immediately precede the fishbone bursts, suggesting a correlation). These observations are consistent, for example, with a model where the CAE are localized far off-axis and the TAE are primarily driven by, and cause the loss of, core fast ions.

In Fig. 3 is shown a spectrogram of the Mirnov data from Fig. 2. The frequency of the modes in the TAE bursts is seen to be roughly in the range from 80 to 130 kHz. The toroidal mode numbers of each of the bursts are indicated by colors as described in the figure caption. The mode numbers are calculated from Fourier transform phases on  $\approx 0.5$  ms intervals using a toroidal array of 12 Mirnov coils. Also shown is the time evolution of the estimated core TAE frequency,  $V_{Alfvén}(0)/4\pi q R$ , together with the approximate Doppler shifted frequencies for the dominant toroidal mode numbers  $n=2$  and  $n=3$ . Modes with toroidal mode numbers ranging from  $n=2$  up to  $n=5$  are present. The Doppler shift is calculated from the interim charge exchange recombination spectrum diagnostic<sup>55</sup> measurement of the plasma rotation near the core. The spacing of the dominant TAEs is roughly consistent with the spacing expected from the Doppler shift, although the gap is calculated to be wide, and this might be coincidental.

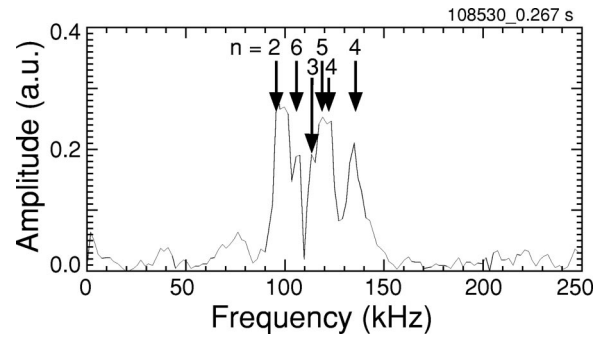


FIG. 4. Spectrum of magnetic fluctuations during TAE burst with toroidal mode numbers indicated. (Same shot as Figs. 2 and 3.)

Each final burst is seen to consist of several modes with toroidal mode numbers ranging from  $n=2$  to  $n=6$ . This is shown more clearly for the burst at 0.283 s in Fig. 4. The spectrum of the time derivative of the magnetic fluctuation contains at least six modes. The mode numbers of the primary spectral components are indicated in the figure. Note that at least two peaks share the same mode number,  $n=4$ . The shortness of the burst precludes better spectral resolution, and there could be additional unresolved modes in the large peaks. The presence of multiple modes may also enhance the fast ion transport.<sup>49,54</sup>

Figure 5 shows the gap structure for the  $n=2$  mode, calculated with NOVA<sup>56</sup> based on the measured density profile and the  $q$  profile inferred from EFIT. The gap is very wide at large minor radius, as is characteristic for low aspect ratio tokamaks. In this example the gap becomes quite narrow near the axis as  $q(0) \approx 2$ . However, there is considerable uncertainty in the  $q$  profile and as little as a 10% change in  $q(0)$  will open the gap. Improved resolution will have to wait for new diagnostics. The predicted range of TAE frequencies ( $\approx 40-70$  kHz) is in reasonable agreement with the observed frequency range given the range of potential Doppler-shift corrections (codes which can predict the Doppler-shift in the presence of sheared rotation do not yet exist).

A wide range of NSTX equilibria has previously been analyzed for stability to TAE<sup>49</sup> and their effect on fast ion transport has been simulated with a guiding center code ORBIT.<sup>57</sup> Instability to multiple TAE was found for equilibria with  $q(0)$  ranging from less than 1 to greater than 2 and a

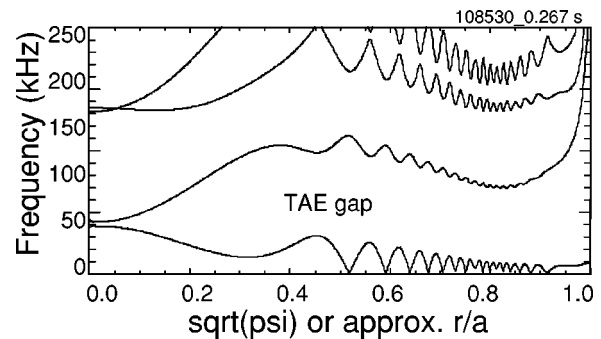


FIG. 5. Gap structure calculated with NOVA-K for the  $n=2$  modes and parameters from the same time in the discharge as in Fig. 4.

range of density profile shapes. As suggested by the above-mentioned experimental results, in the simulations the presence of multiple (2) modes and an elevated  $q(0)$  enhanced the fast ion loss rate. The inferred levels of loss in the experiment are, however, higher than in the simulations. The guiding center approximation may not be adequate in the ST geometry and a nonperturbative code may be necessary to properly model the TAE instability. Further, the effectiveness of the TAE in causing fast ion loss also depends on the radial extent of the modes; a “sea” of TAE extending across the full plasma cross section might be much more effective in ejecting fast ions from the plasma than a few, more localized, modes.

## B. “Fishbone” induced losses

Chirping modes are seen in NSTX with frequencies beginning at over 100 kHz and chirping down to a few kilohertz on a time scale of milliseconds. The time scale for the chirping, together with the short repetition time, suggests that these are fast ion driven instabilities which are affecting the beam fast ion distribution. The bursting and chirping are qualitatively similar to the behavior of the fishbone mode seen in conventional-aspect ratio tokamaks. However, the frequency range of the chirps can be much larger than for conventional fishbone modes and the toroidal mode number is not necessarily unity, but can be as large as  $n = 5$ .

The chirping modes on NSTX can be qualitatively separated into two groups. The first group, herein referred to as Type II (classic fishbones would be Type I), consists of modes with frequency characteristics similar to those of the original fishbone mode. However, the frequency chirp starts near the upper range of fast ion bounce, rather than precession, frequencies and approaches zero in the plasma frame at the low frequency end. The downward chirp can be accompanied by fast ion losses, inferred from a transient drop in the neutron rate, directly measured increases in fast ion losses, and bursts of D-alpha as the fast ions hit the plasma facing components. On NSTX, the repetition rate for this type of mode can range from essentially isolated events to periods as short as 5–10 ms. Unlike the original fishbone instability, this mode often occurs when the inferred  $q(0)$  is well above unity. Further, the mode is not limited to a toroidal mode number of  $n = 1$ , but ranges up to at least  $n = 5$ .

The second group of fishbone-type modes (referred to as Type III) tends to have higher frequencies, is generally  $n = 1$ , and has a smaller frequency range in the chirps. They are also much more common, occurring in virtually every NSTX NBI heated plasma. They begin shortly after the start of NBI heating during the current ramp and end, typically, about the time the current flattop starts. As yet, there has been no detected impact of these modes on fast ion confinement. As these modes overlap the first toroidal Alfvén eigenmode gap, they may also be a form of resonant toroidal Alfvén eigenmode (rTAE) or energetic particle mode (EPM).

Most of the features of the above-described fishbone-type modes can be seen in the spectrogram shown in Fig. 6. Here the fitted toroidal mode numbers are again indicated by colored contours. The Type III fishbones are the black band

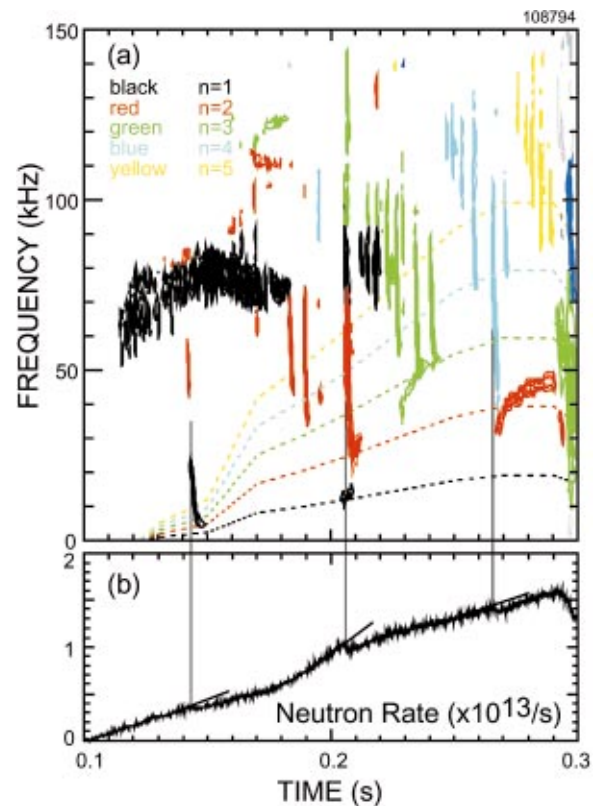


FIG. 6. (Color) Mirnov coil spectrogram showing Types II and III fishbone activity, correlated with drops in the neutron emission (6b). Plasma current is 1 MA, toroidal field is 4.5 kG, neutral beam heating power 1.7 MW at 80 kV. (The mode numbers are indicated by color, black— $n = 1$ , red— $n = 2$ , green— $n = 3$ , blue— $n = 4$ , and yellow— $n = 5$ .)

between 0.1 and 0.2 s and roughly between 50 and 90 kHz. The individual bursts of these modes are so close together that they are not resolved. The black dashed line shows the plasma rotation measured by a charge-exchange recombination diagnostic<sup>55</sup> at a major radius of 1.3 m, or about the  $q = 1.5$  radius.

The Type II fishbone bursts occur less frequently and often evolve throughout the shot with the toroidal mode increasing from  $n = 1$  up to  $n = 5$ . The first Type II fishbone occurs between roughly 0.14 and 0.15 s. During this approximately 10 ms interval, the mode frequency drops from about 25 to about 5 kHz. The mode number is  $n = 1$ . The  $q(0)$  is inferred by an EFIT equilibrium calculation to be approximately 1.8. Three or four fishbones with  $n = 2$  (red) then follow during the period from 0.18 to 0.21 s. This sequence continues as the toroidal mode numbers increase through  $n = 3$  (green),  $n = 4$  (blue), and  $n = 5$  (yellow).

Below the spectrogram is shown the time evolution of the neutron flux. The first Type II fishbone results in a discernible pause in the rise of the neutron rate. Only this fishbone, and the fishbones at 0.205 and 0.265 s cause measurable drops in the neutron rate. Thus, many of these Type II fishbones also had little impact on the neutron rate.

While the edge magnetic fluctuation level is at best an indirect measure of the internal mode amplitude, there is a correlation between the impact on the neutron rate and the edge magnetic fluctuation amplitude in this shot. In Fig. 7 is

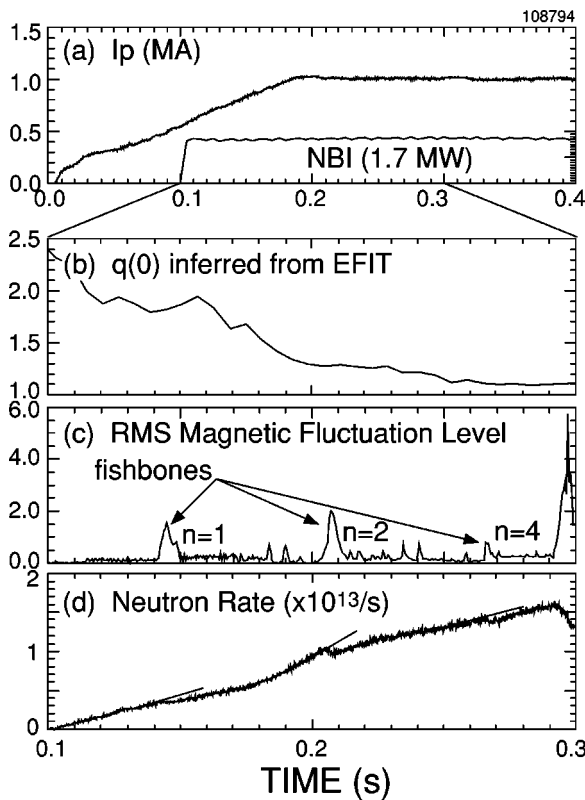


FIG. 7. Waveforms showing the evolution of a NSTX discharge from Fig. 6 with fishbone activity. (a) Plasma current and neutral beam heating power, (b)  $q(0)$  inferred from EFIT, (c) rms magnetic fluctuation level with the  $n=1$ ,  $n=2$ , and  $n=4$  fishbones correlated with neutron drops indicated, (d) neutron emission. (Fluctuation burst after 0.29 s is an IRE-like event, not fishbone.)

shown the rms magnetic fluctuation level and again the time evolution of the neutron rate. Clearly the two largest modes, as measured by Mirnov coils on the outboard midplane, are those which result in two of the three significant neutron rate dips. Those fishbones which had the strongest effect were also those that swept to the lowest frequencies. While there is some agreement between the low end of the fishbone chirp and the bulk plasma rotation frequency, it is clearly not exact. As there is substantial shear in the plasma rotation, accurate modeling of the expected mode frequencies will present something of a challenge.

During the sequential evolution of the toroidal mode number from  $n=1$  up to  $n=5$  the current profile continues to peak, with  $q(0)$  decreasing from somewhere near  $q(0) \approx 2$  at the time of the  $n=1$  fishbone, to  $q(0) \approx 1$  by the time of the  $n=5$  fishbones. During this time, the plasma density increases from 2 to  $3 \times 10^{19}/\text{m}^3$ , which may affect the fast ion distribution. Thus it is also possible that the mode number evolution reflects an evolution in the fast ion distribution.

Some indication of the internal structure of the fishbone modes is visible in the soft x-ray data. In Fig. 8 are shown the soft x-ray traces from a pinhole camera<sup>58</sup> observing the plasma in the nominal horizontal direction. In Fig. 8(a), the individual traces are auto-scaled and graphed at their approximate tangency (midplane minor) radius through the time period of the fishbone which results in the first large

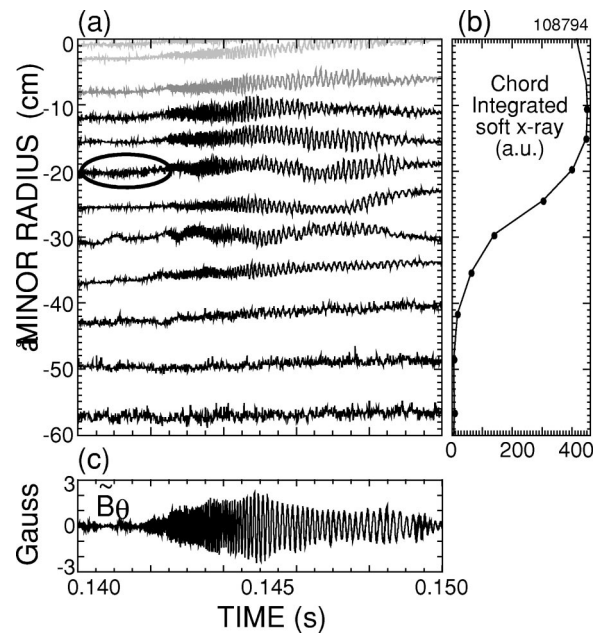


FIG. 8. Soft x-ray camera and Mirnov coil data during Type II fishbone event shown in Figs. 6 and 7. (a) Auto-scaled soft x-ray camera traces plotted at their approximate minor radius positions. Oval indicates Type III fishbones. (b) Chord integrated soft x-ray profile at 0.145 s. (c) Magnetic fluctuation level during this time period in gauss.

drop in neutron emission. There is an inversion in the oscillations between 0.2 and 0.25 m in minor radius which is most likely due to a hollow soft x-ray emissivity profile, peaked at this radius. The much weaker Type III fishbones can also be seen in this figure before and after the Type II fishbone. The bandwidth of the soft x-ray camera is  $>100$  kHz, so the higher frequency modes are not suffering from attenuation. However, if the poloidal wavelength of the Type III fishbones was much shorter than the Type II, the chord integration could reduce the apparent amplitude.

Interpretation of soft x-ray data is difficult due to the complicated dependence on plasma parameters and the chord integration. Figure 8(b) shows the chord integrated soft x-ray profile. There is a strong gradient in the chord integrated emissivity profile between roughly  $r=0.15$  m and  $r=0.45$  m. Within this range the soft x-ray data will be more sensitive to displacements than in regions where the emissivity profile is flatter.

For comparison, Fig. 9 (in the same format as Fig. 8) shows the  $n=2$  fishbone at 0.195 s. In this case the mode amplitude in the soft x-ray signal appears much weaker than for the example in Fig. 8, while the amplitude on the Mirnov coil is only slightly smaller, suggesting that the radial structure of the mode is different. The fluctuations from the fishbone are circled in red. The radial location of the mode appears similar; however, as the soft x-ray emissivity drops precipitously toward the plasma periphery, it is not clear that there is sufficient sensitivity in the edge channels to conclude that the mode amplitude is weaker near the edge.

The fishbone event at 0.205 s is more complex. The fishbone appears to be triggered by a small sawtooth-like event. In this case it is possible that some of the fast ion losses are due directly to the sawtooth event. The soft x-ray

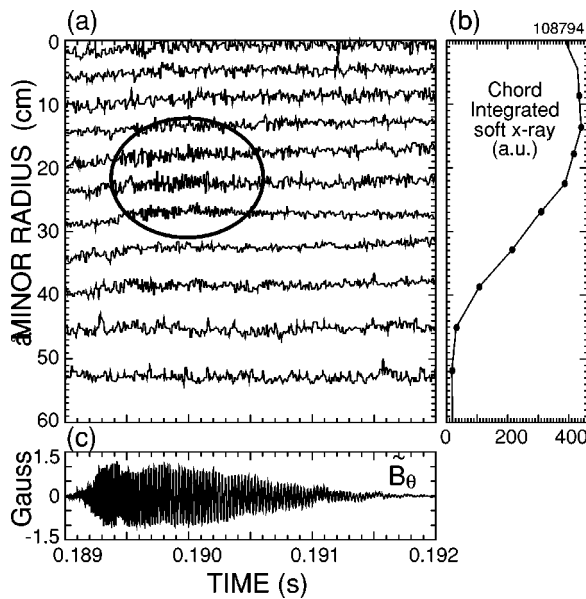


FIG. 9. Soft x-ray camera and Mirnov coil data showing an  $n=2$  Type II fishbone event from Figs. 6 and 7. (a) Soft x-ray traces at their approximate radial locations showing a “weak” fishbone mode. (b) Soft x-ray profile at 0.1905 s. (c) Integrated signal from Mirnov coil over this time interval in gauss.

emissivity is flat or hollow in the core region, precluding detailed reconstruction of the event, however the sawtooth event has a lower frequency precursor. In Fig. 10 are shown the soft x-ray traces from the lower camera up to the onset of the fishbone mode. A low frequency mode at 7 kHz (and  $n=1$  on the Mirnov array) is growing until  $\approx 0.2054$  s. During the final growth, an increase in the soft x-ray emissivity is seen on the soft x-ray chords between  $\approx 20$  and  $\approx 40$  cm. Soft x-ray emissivity profiles from before and after this event

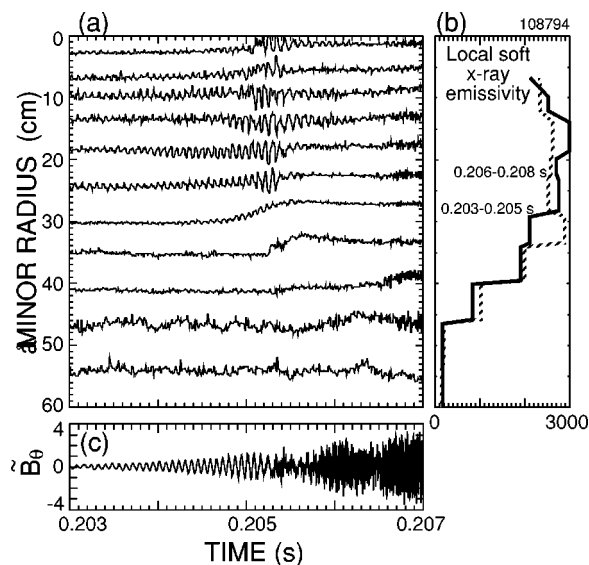


FIG. 10. Soft x-ray traces showing a sawtooth-like event, together with a low frequency precursor followed by a fishbone burst. (a) Auto-scaled soft x-ray traces at their approximate minor radial positions, (b) inverted soft x-ray profiles from before and after the event at 0.205 s showing the soft x-ray emissivity drops in the core and increases outside, (c) un-integrated Mirnov coil signal through this event.

are shown in Fig. 10(b). The emissivities are inferred by inverting the chord integrated data as constrained by the EFIT equilibria. The inversions suggest that the emissivity drops in the core region and increases outside a minor radius of about 0.28 m, i.e., consistent with a sawtooth-like event. EFIT, however, calculates  $q(0) \approx 1.3$  at this time and the event is much weaker than the sawteeth normally seen on NSTX.

In Fig. 11 is shown a spectrogram of a 0.8 MA shot with 6 MW (at 90 kV) of neutral beam heating power. Again, fishbones, with a somewhat longer period, are causing 20% transient drops in the neutron rate. In this case the later fishbones between 0.24 and 0.29 s have a toroidal mode number of  $n=3$  whereas the earlier fishbones are a combination of  $n=2$  and  $n=1$  modes. The earlier fishbones, while reaching similar fluctuation amplitudes on Mirnov coils and soft x rays, had a much smaller effect on the neutron rate. That could mean either that the structure of the  $n=3$  mode interacted more effectively with the fast ion distribution or that the  $n=2$  modes interacted primarily with lower energy fast ions whose loss did not as seriously impact the neutron rate. More detailed studies with improved diagnostics, coupled with advanced theoretical models will be required to sort these issues out.

In Fig. 11(c) is shown the D-alpha emission from the upper divertor region. The drop in D-alpha at 0.26 s indicates an  $H$ -mode transition. In this shot, and many others, there is a fishbone at or just preceding the  $H$ -mode transition, suggesting that fishbones could help to trigger an  $H$  mode (e.g., by expelling fast ions which charges the plasma up and induces rotation<sup>59</sup>). This conjecture is bolstered by the observations that the two fishbones preceding the  $H$ -mode transition result in D-alpha drops, suggestive of dithering  $H$  modes. The fishbone following the  $H$ -mode transition is correlated with a small spike in D-alpha, as in the bursting TAE examples. However, fishbone bursts are not as clearly correlated with D-alpha bursts, even fishbone bursts with large neutron drops. This may indicate that the fast ions are lost to a different, unobserved, part of the machine.

For many of the chirping modes seen in NSTX<sup>34,43</sup> and START (42) the fast ion precession frequency is too low to effectively drive modes at the observed frequencies. As is shown in Ref. 43, the drive for the mode can be through a bounce, rather than precession resonance. In this paper a ballooning representation for the mode dispersion relation was used to allow for an analytic solution. For the bounce resonance drive to be effective, a large average bounce angle for the fast ion distribution function is necessary, as is the case for NSTX.<sup>34,43</sup> For NSTX parameters, the bounce resonance comes primarily with the intermediate energy (<40 kV) beam ions, thus the small effect on neutron rate would not be surprising. However, in a fusion reactor where the fast ion source is more isotropic, the bounce resonance could occur with, and transport the highest energy particles.

### C. Induced losses in the presence of combined TAE and fishbone modes

TAE instabilities often co-exist with fishbone modes, and under some circumstances the TAE bursts also appear to

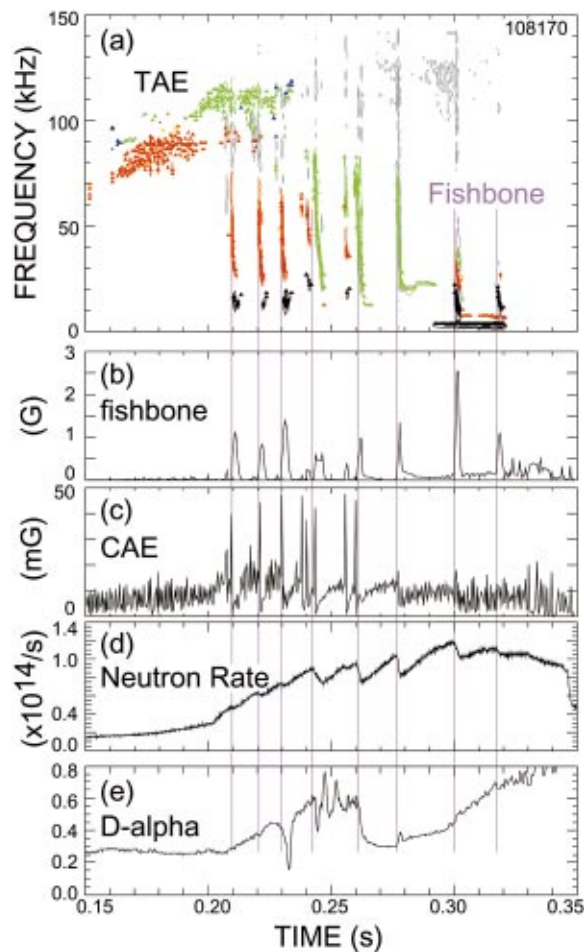


FIG. 11. (Color) Mirnov spectrogram showing fishbone bursts. Plasma current 800 kA, toroidal field 4 kG, neutral beam heating power 3.2 MW at 80 kV. Contour colors indicate inferred toroidal mode numbers; black is  $n = 1$ , red is  $n = 2$ , green is  $n = 3$ , cyan is  $n = 4$ , yellow is  $n = 5$ , and blue is  $n = 6$ . (b) rms fluctuation level in gauss over the frequency range 10–90 kHz showing the amplitude of the fishbone modes, (c) rms fluctuation level in gauss over the frequency range 500–1200 kHz showing compressional Alfvén eigenmode bursts, (d) neutron emissivity showing 20% drops at  $n = 3$  fishbone bursts, but only weak drops at earlier bursts, (e) D-alpha emission drops during fishbones immediately prior to H-mode transition, small spike for fishbone after transition.

trigger fishbones. In Fig. 12(a) is shown a spectrogram of a shot in which many of the fishbones are apparently triggered by TAE bursts. Below the spectrogram is shown the neutron evolution [Fig. 12(b)] and in Fig. 12(c) the envelope of the magnetic fluctuation level for the frequency bands 5–50 kHz (fishbones) and 70–110 kHz (TAE). The drop in the neutron rate is as large as 20% for the later bursts, and the repetition period is approximately 10 ms, or roughly one-third of the fast ion slowing down time. The effect of periodic losses of fast ions can be simply estimated, based on the assumption of short periodic bursts of losses, a constant replenishment rate, and exponential slowing down time for the fast ions. For the roughly 10 ms period of 15% losses, the effect on the “steady state” fast ion population suggests that in steady state, such modes would reduce the fast ion population by  $\approx 40\%$ .

In the latter phase of long pulse, high beta discharges, the fishbones often have multiple toroidal mode numbers

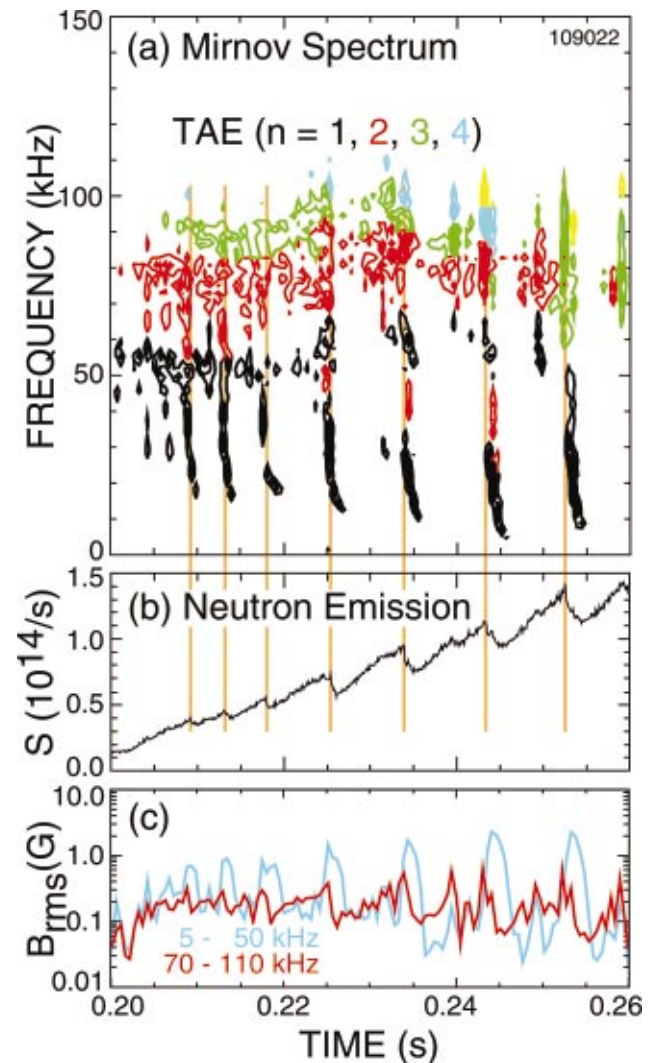


FIG. 12. (Color) Effect of combined TAE and fishbone mode bursts on neutron emissivity. Plasma current 800 kA, toroidal field 4.5 kG, neutral beam heating power 6.1 MW at 90 kV. (a) Spectrogram of Mirnov coil showing fishbones and bursting TAE (black, red, green, blue, yellow correspond to  $n = 1, 2, 3, 4, 5$ , respectively), (b) neutron emission showing up to 20% drops at the combined MHD bursts, (c) rms magnetic fluctuation levels in the 5–10 kHz (blue) band and 70–110 kHz band (red) showing fishbone amplitude and TAE amplitude evolution, respectively.

( $n = 1$  through  $n = 3$  or 4). The fast ion losses from these events can be substantial; neutron drops as large as 25% have been seen (Fig. 13). For these fishbones, large bursts in the neutral particle analyzer (NPA)<sup>60,61</sup> signal have been observed coincident with the fishbone chirps on the Mirnov data. An example, from the latter half of the discharge shown in Fig. 12, is shown in Fig. 13. Such bursts have been observed over a wide range in the NPA tangency radii of  $R_{\text{tan}} = 15\text{--}92$  cm.

The fishbone-induced bursts are observed at all energies in the neutral beam ion spectrum “chirp” (sweep downward) in energy as illustrated in Fig. 14. Shown are the energetic ion spectra with 1 ms time resolution for 1 ms before the fishbone (black curve), the first (red curve) and second (blue curve) millisecond of the fishbone chirp, and 1 ms after the end of the fishbone (purple curve). During the first millisecond of the fishbone, the entire energy spectrum increases by

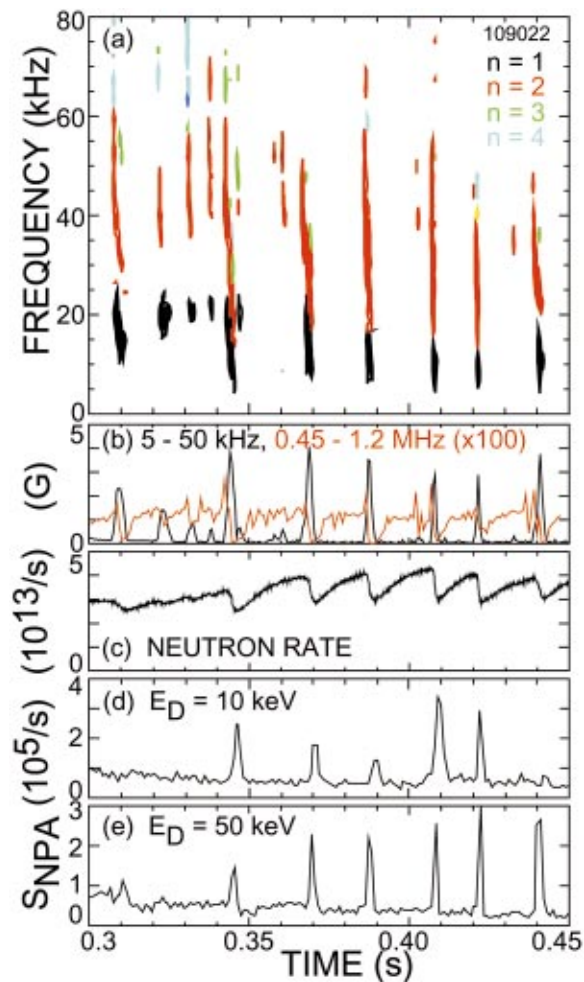


FIG. 13. (Color) Fishbone modes with toroidal mode numbers of  $n=1$  and  $n=2$  in the latter half of the plasma discharge shown in Fig. 12. (a) Spectrogram of Mirnov coil, black contours are  $n=1$  modes, red are  $n=2$ . (b) rms fluctuation levels in the frequency bands 5–50 kHz (black) and 450–1200 kHz (red) showing the amplitude evolution of the fishbone and CAE, respectively (the CAE band is scaled by 100). (c) Neutron rate showing  $\approx 25\%$  drops in emissivity at each fishbone burst, (d) neutral particle analyzer signal showing 10 keV deuterium channel, (e) neutral particle analyzer signal showing 50 keV deuterium channel.

approximately two e-foldings or a factor of 5–10. During the following millisecond, the spectrum above  $\sim E_b/2$  approaches the pre-fishbone level (i.e., the ion loss terminates) while ions below  $E_b/2$  continue to be elevated (ion loss continues). In the millisecond after the fishbone, the spectrum above  $E_b/2$  is depleted by  $\sim 25\%$  relative to the pre-fishbone level, a loss in energetic ion population that is consistent with the observed drop in the neutron yield.

With occasional exceptions, bursts in the NPA signal due to fishbones are not correlated with spikes in the D-alpha emission or with features in the ion loss signal from the iFLIP lost ion diagnostic. In conjunction with observation of fishbone-induced enhancement of the NPA signal at all energies, this argues that the fishbones cause redistribution of a fraction of the NB ion distribution from the plasma core to more peripheral regions where the higher background neutral signal leads to the observed burst in the NPA signal. To date, no effect has been observed on the thermal deuterium ion spectra due to fishbone activity.

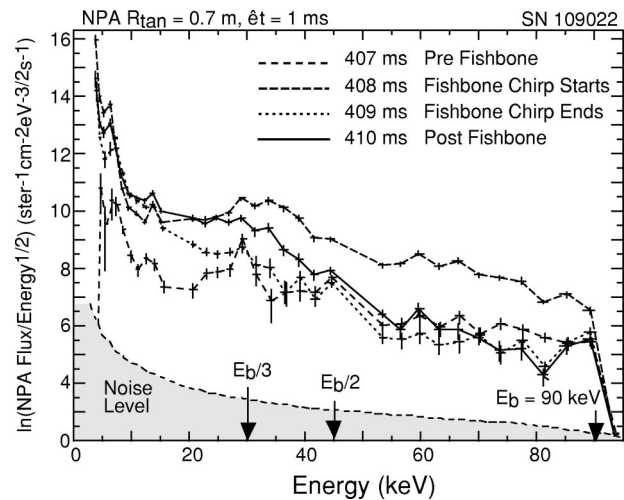


FIG. 14. Fast ion spectra with full, half, and third energy levels marked. Four time intervals are shown through a single fishbone event.

### III. DISCUSSION

Previous studies had predicted that STs might be strongly unstable to TAE instabilities, so the observation of TAE in NSTX was not a surprise. The discovery of significant fast ion losses resulting from TAE instabilities provides motivation to improve the theoretical tools for predicting the impact of these modes in proposed ST reactors. Likewise, the discovery that the fishbone-like bursts could cause significant fast ion transport should provide impetus to theoretical efforts to understand these modes. The realization that these modes could be driven through a bounce, rather than precession resonance in the ST implies that such a drive mechanism might also work in some operational regimes of conventional tokamak reactors. The observation of fishbone-like modes with  $m, n \neq 1$  further suggests that the bounce-resonance drive might be quite effective.

The estimated impact on fast ion confinement of the strongly bursting TAE, the fishbone-like instability, or a combination of these two modes can be quite significant. For the most extreme examples, the fishbone bursts, in steady state, would reduce the fast ion population by 50% (cf., Fig. 11 with 20% neutron drops every 10 ms). Since fast ion loss will directly impact the ignition margin in reactors, it is important to understand the scaling of the loss. Just as important as the impact on ignition margin is the impact of the fast ions on the reactor first wall. In reactors, the fast ion population is measured in 100's of MJ, thus it is also important to determine how localized in time and space the power deposition is from the fast ion loss.

The present set of NSTX data is not adequate to address the scaling of the losses to other (e.g., reactor) regimes for several reasons. First, the present range of NSTX parameters is relatively small, and the measurement of one of the most important parameters, the current profile, is uncertain. Second, the ability to directly measure the effect of the modes on the fast ion distribution is limited. The primary diagnostic at present is the measurement of the neutron flux, which only measures loss of the most energetic fast ions and is not sensitive to redistribution of fast ions within the plasma, or of losses of intermediate energy fast ions. Finally, the TAE and

fishbones generally co-exist, complicating the understanding of the mechanisms for fast ion loss. The principal diagnostic for measuring the mode amplitude is the array of Mirnov coils, which provide at best an indirect measure of the mode amplitude. Diagnostics which can measure the internal structure of the mode do not work well in plasmas where large fast ion losses are most commonly seen, i.e., in  $H$  modes with flat density profiles. Experiments are being planned to explicitly address the scaling issue, but must await run time, and would ideally be performed after the addition of a current profile diagnostic. Scaling to other regimes must, at present, rely on imperfect theoretical models for the instabilities and fast ion transport.

The observation of bursting TAE causing fast ion losses is not new. The first observations of TAE in a conventional aspect ratio plasma were accompanied by fast ion losses similar in magnitude to those observed here.<sup>2</sup> However, reactor versions of conventional aspect ratio tokamaks are high field (5–10 T), high current (up to 20 MA) with large minor radius (several meters). In this regime, the TAE activity was predicted, at worst, to affect the fast ion population diffusively. This is not so clearly the case for a reactor concept like ARIES-ST.<sup>37</sup> The normalized alpha Larmor radius is somewhat smaller than on NSTX (0.04 compared to 0.2), but not much smaller than that of conventional tokamaks (0.06–0.09) where substantial TAE induced losses were seen.<sup>6,62</sup> Further, the parameter regime where the bursting TAE are observed in NSTX, i.e., with broad density (pressure) profile and elevated  $q$  on axis, is the regime proposed for long pulse, high bootstrap fraction ST operation.

The “fishbones” have been identified as a type of “energetic particle mode” (EPM), based largely on the strong frequency chirping. Energetic particle modes are strongly driven instabilities whose frequency is determined by the optimized resonance condition with the fast ion distribution. Because the mode frequency is not set by equilibrium plasma properties (such as density or magnetic field strength), the frequency can change as quickly as the mode can modify the fast ion distribution. The original fishbone model, developed to fit the observations made on PDX, was a resonance of the mode with the precession-drift of the fast ions.<sup>1–4</sup> The peak in the energy transfer (from fast ions to mode) occurred at the highest frequency with the most energetic ions. As the most energetic ions were lost, the optimum resonance frequency dropped, coupling to lower energy ions. Thus, a characteristic of the fishbones was a fast downward chirp in frequency. The bursting character followed the classic predator–prey relation.<sup>16</sup> Although the fishbones on NSTX have significant differences from classic fishbones, they retain two features of the classic fishbones, namely the strong chirping and the bursting character.

The classic fishbone (Type I) was a predominantly  $m = 1$ ,  $n = 1$  instability in plasmas with  $q(0) < 1$ . In NSTX the fishbones have been seen with toroidal mode numbers from  $n = 1$  to  $n = 5$ . They are also most commonly seen in plasmas with  $q(0)$  well above unity, implying  $m > 1$ . Because of the high beta and low aspect ratio the precession frequency in a ST can be quite small, and in some cases reverses direction. Thus, it is believed that the resonance drive in NSTX is

through the fast ion bounce resonance.<sup>34,43</sup> For this resonance condition to be strong, the average bounce angle (angle of banana turning points) must be large. For many beam heated shots on NSTX there is a large population of fast ions, not necessarily the most energetic, which have large bounce angles. A similar situation is expected in fusion-alpha heated reactors where the alpha population is intrinsically isotropic. This resonance condition should still retain the feature that the energy transfer rate is proportional to the mode frequency; the modes should still appear first with high frequency, and chirp down as the fast ions are lost.

The discovery of these bounce-resonance fishbones on NSTX is significant in that the classic fishbones were predicted to be stable in conventional aspect ratio fusion reactors (and NSTX) as the high beta resulted in small precession frequencies (i.e., weak drive). The proposed bounce-resonance drive model requires further comparison to NSTX results before it can be applied to reactor-relevant conditions. The observation of bursting TAE correlated with fast ion losses also underscores the importance of extending TAE physics models to the ST regime.

#### IV. SUMMARY

Clear evidence of fast ion losses has been seen in conjunction with at least two forms of fast ion driven instabilities in the spherical torus NSTX. In  $H$ -mode plasmas with elevated  $q$  on axis, bursting TAE causing 10%–15% neutron drops were seen. From the burst frequency and estimated slowing down time, these modes in steady state would result in an average 40% reduction of the fast ion population. This regime is similar to that envisioned for a bootstrap-current-driven ST reactor. The dimensionless parameters of the alpha particles are similar to those of the neutral beam ions in NSTX, although the beam ion distribution also includes substantial half and third energy components, and is less isotropic than the fusion alpha distribution is expected to be. Further theoretical modeling is required to evaluate the importance of TAE instabilities in ST reactors.

Bursting, chirping modes were also seen to cause fast ion losses at rates up to 20% fast ion loss per burst. This would correspond to as much as a 50% reduction in fast ion population in steady state. These modes differ substantially from the normal fishbone modes seen in conventional aspect ratio tokamaks. Toroidal mode numbers for these modes have been seen between  $n = 1$  and  $n = 5$ . They are typically seen when the  $q(0)$  is believed to be well above unity. Finally, the modes are often present when the beam-ion precession frequency is nearly zero—a condition generally assumed to be stable to fishbones. A theoretical model for these modes has been separately proposed.<sup>34,43</sup>

#### ACKNOWLEDGMENTS

We are grateful to the NSTX team for supporting these experiments. We also wish to acknowledge very useful discussions with Dr. S. Jardin. The help of Dr. M.G. Bell and Dr. S. Kaye in the preparation of this manuscript are also greatly appreciated.

This work is supported by U.S. DOE Contract No. DE-AC02-76CH03073.

- <sup>1</sup>K. M. McGuire, R. Goldston, M. Bell *et al.*, Phys. Rev. Lett. **50**, 891 (1983).
- <sup>2</sup>R. B. White, R. J. Goldston, K. M. McGuire *et al.*, Phys. Fluids **26**, 2958 (1983).
- <sup>3</sup>L. Chen, R. B. White, and M. N. Rosenbluth, Phys. Rev. Lett. **52**, 1122 (1984).
- <sup>4</sup>W. W. Heidbrink, K. Bol, D. Buchenauer, R. Fonck, G. Gammel, K. Ida, R. Kaita, S. Kaye, H. Kugel, B. LeBlanc, W. Morris, M. Okabayashi, E. Powell, S. Sesnic, and H. Takahashi, Phys. Rev. Lett. **57**, 835 (1986).
- <sup>5</sup>C. Z. Cheng and M. S. Chance, Phys. Fluids **29**, 3695 (1986).
- <sup>6</sup>K. L. Wong, R. J. Fonk, S. F. Paul *et al.*, Phys. Rev. Lett. **66**, 1874 (1991).
- <sup>7</sup>J. R. Wilson, M. G. Bell, H. Biglari, M. Bitter, N. L. Bretz *et al.*, *Proceedings of the 14th International Conference On Plasma Physics and Controlled Nuclear Fusion Research* (IAEA, Vienna, 1992), Vol. I, p. 661.
- <sup>8</sup>K. L. Wong, Plasma Phys. Controlled Fusion **41**, PR1 (1999).
- <sup>9</sup>D. S. Darrow, S. J. Zweben, Z. Chang, C. Z. Cheng, M. D. Diesso, E. D. Fredrickson, E. Mazzucato, R. Nazikian, C. K. Phillips, S. Popovichev, M. H. Redi, R. B. White, J. R. Wilson, and K. L. Wong, Nucl. Fusion **37**, 939 (1997).
- <sup>10</sup>S. J. Zweben, R. V. Budny, D. S. Darrow, S. S. Medley, R. Nazikian, B. C. Stratton, E. J. Synakowski, and G. Taylor, Nucl. Fusion **40**, 91 (2000).
- <sup>11</sup>R. B. White, E. Fredrickson, D. Darrow, M. Zarnstorff, R. Wilson, S. Zweben, K. Hill, Y. Chen, and G. Fu, Phys. Plasmas **2**, 2871 (1995).
- <sup>12</sup>W. W. Heidbrink, E. J. Strait, E. Doyle, G. Sager, and R. T. Snider, Nucl. Fusion **31**, 1635 (1991).
- <sup>13</sup>H. H. Duong, W. W. Heidbrink, E. J. Strait, T. W. Petrie, R. Lee, R. A. Moyer, and J. G. Watkins, Nucl. Fusion **33**, 749 (1993).
- <sup>14</sup>H. H. Duong and W. W. Heidbrink, Nucl. Fusion **33**, 211 (1993).
- <sup>15</sup>E. J. Strait, W. W. Heidbrink, A. D. Turnbull, M. S. Chu, and H. H. Duong, Nucl. Fusion **33**, 1849 (1993).
- <sup>16</sup>W. W. Heidbrink, H. H. Duong, J. Manson, E. Wilfrid, and C. Oberman, Phys. Fluids B **5**, 2176 (1993).
- <sup>17</sup>M. Saigusa, H. Kimura, S. Moriyama, Y. Neyatani, T. Fujii, Y. Koide, T. Kondoh, M. Sato, M. Nemoto, Y. Kamada, and JT-60 team, Plasma Phys. Controlled Fusion **37**, 295 (1995).
- <sup>18</sup>H. Kimura, M. Saigusa, S. Moriyama, T. Kondoh, Y. Neyatani, T. Ozeki, T. Nishitani, Y. Kusama, T. Fujii, M. Sato, M. Nemoto, K. Tobita, and C. Z. Cheng, Phys. Lett. A **199**, 86 (1995).
- <sup>19</sup>M. Saigusa, H. Kimura, Y. Kusama, G. J. Kramer, T. Ozeki, S. Moriyama, T. Oikawa, Y. Neyatani, and T. Kondoh, Plasma Phys. Controlled Fusion **40**, 1647 (1998).
- <sup>20</sup>G. Kremer, M. Iwase, Y. Kusama *et al.*, Nucl. Fusion **40**, 1383 (2000).
- <sup>21</sup>K. Tobita, Y. Kusama, K. Shinohara *et al.*, Fusion Sci. Technol. **42**, 315 (2002).
- <sup>22</sup>S. Ali-Arshad and D. J. Campbell, Plasma Phys. Controlled Fusion **37**, 715 (1995).
- <sup>23</sup>A. Fasoli, D. Borba, G. Bosia, D. J. Campbell, J. A. Dobbing, C. Gormezano, J. Jacquinet, P. Lavanchy, J. B. Lister, P. Marmillod, J. M. Moret, A. Santagiustina, and S. Sharapov, Phys. Rev. Lett. **75**, 645 (1995).
- <sup>24</sup>A. Fasoli, D. Borba, C. Gormezano, R. Heeter, A. Jaun, J. Jacquinet, W. Kerner, Q. King, J. B. Lister, S. Sharapov, D. Start, and L. Villard, Plasma Phys. Controlled Fusion **39**, 287 (1997).
- <sup>25</sup>A. Fasoli, J. A. Dobbing, C. Gormezano, J. Jacquinet, J. B. Lister, S. E. Sharapov, and A. Sibley, Nucl. Fusion **36**, 258 (1996).
- <sup>26</sup>C. Z. Cheng, N. N. Gorelenkov, and C. T. Hsu, Nucl. Fusion **35**, 1639 (1995).
- <sup>27</sup>F. Zonca and L. Chen, Phys. Plasmas **3**, 323 (1996).
- <sup>28</sup>E. D. Fredrickson, M. G. Bell, R. V. Budny, Z. Chang, C. Z. Cheng, G. Y. Fu, E. Mazzucato, R. Nazikian, A. T. Janos, K. M. McGuire, R. Majeski, C. K. Phillips, G. Schilling, G. Taylor, and J. R. Wilson, Nucl. Fusion **35**, 1457 (1995).
- <sup>29</sup>S. Bernabei, M. G. Bell, R. V. Budny, E. D. Fredrickson, N. N. Gorelenkov, J. C. Hosea, R. Majeski, E. Mazzucato, C. K. Phillips, G. Schilling, and J. R. Wilson, Phys. Rev. Lett. **84**, 1212 (2000).
- <sup>30</sup>S. Bernabei, R. V. Budny, E. D. Fredrickson *et al.*, Nucl. Fusion **41**, 513 (2001).
- <sup>31</sup>S. Bernabei, M. G. Bell, R. Budny, D. Darrow, E. D. Fredrickson, N. Gorelenkov, J. C. Hosea, R. Majeski, E. Mazzucato, R. Nazikian, C. K. Phillips, J. H. Rogers, G. Schilling, R. White, J. R. Wilson, F. Zonca, and S. Zweben, Phys. Plasmas **6**, 1880 (1999).
- <sup>32</sup>M. Ono, S. M. Kaye, Y.-K. M. Peng *et al.*, Nucl. Fusion **40**, 557 (2000).
- <sup>33</sup>E. D. Fredrickson, N. Gorelenkov, C. Z. Cheng, R. Bell, D. Darrow, D. Johnson, S. Kaye, B. LeBlanc, J. Menard, S. Kubota, and W. Peebles, Proceedings of 28th EPS Conference on Controlled Fusion and Plasma Physics, Funchal, 2001, ECA Vol. 25A, p. 1001.
- <sup>34</sup>E. D. Fredrickson, C. Z. Cheng, L. Chen, D. Darrow, N. N. Gorelenkov, D. Johnson, S. Kaye, S. Kubota, J. Menard, and R. B. White, Proceedings of 29th EPS Conference on Controlled Fusion and Plasma Physics, Montreux, 2002 (European Physical Society, Geneva, 2002), ECA Vol. 26B, P-1.104.
- <sup>35</sup>E. D. Fredrickson, N. Gorelenkov, C. Z. Cheng, R. Bell, D. Darrow, D. Johnson, S. Kaye, B. LeBlanc, J. Menard, S. Kubota, and W. Peebles, Phys. Rev. Lett. **87**, 145001 (2001).
- <sup>36</sup>E. D. Fredrickson, N. N. Gorelenkov, C. Z. Cheng, R. Bell, D. Darrow, D. Gates, D. Johnson, S. Kaye, B. LeBlanc, D. McCune, J. Menard, S. Kubota, and W. Peebles, Phys. Plasmas **9**, 2069 (2002).
- <sup>37</sup>S. C. Jardin, C. E. Kessel, J. Menard, T. K. Mau, R. Miller, F. Najmabadi, V. Chan, L. Lao, Y. R. Linliu, R. L. Miller, T. Petrie, P. Politzer, and A. D. Turnbull, "Physics bias for a spherical torus power plant," Fusion Eng. Des. (to be published).
- <sup>38</sup>R. Kaita, R. B. White, A. W. Morris, E. D. Fredrickson, K. M. McGuire, S. S. Medley, T. J. Murphy, and S. D. Scott, Phys. Fluids B **2**, 1584 (1990).
- <sup>39</sup>M. F. F. Nave, D. J. Campbell, E. Joffrin, F. B. Marcus, G. Sadler, P. Smeulders, and K. Thomsen, Nucl. Fusion **31**, 697 (1991).
- <sup>40</sup>W. W. Heidbrink, Plasma Phys. Controlled Fusion **37**, 937 (1995).
- <sup>41</sup>W. W. Heidbrink, E. M. Carolipio, R. A. James, and E. J. Strait, Nucl. Fusion **35**, 1481 (1995).
- <sup>42</sup>K. G. McClements, M. P. Gryaznevich, S. E. Sharapov, R. J. Akers, L. C. Appel, G. F. Counsel, C. M. Roach, and R. Majeski, Plasma Phys. Controlled Fusion **41**, 661 (1999).
- <sup>43</sup>E. D. Fredrickson, L. Chen, and R. B. White, "Bounce precession fishbones in the National Spherical Torus Experiment," Nucl. Fusion (submitted).
- <sup>44</sup>S. M. Mahajan and D. W. Ross, Phys. Fluids **26**, 2561 (1983).
- <sup>45</sup>B. Coppi, S. Cowley, R. Kulsrud, P. Detragiache, and F. Pegoraro, Phys. Fluids **29**, 4060 (1986).
- <sup>46</sup>N. N. Gorelenkov and C. Z. Cheng, Nucl. Fusion **35**, 1743 (1995).
- <sup>47</sup>N. N. Gorelenkov, C. Z. Cheng, E. Fredrickson, E. Belova, D. Gates, S. Kaye, G. J. Kramer, R. Nazikian, and R. B. White, Nucl. Fusion **42**, 977 (2002).
- <sup>48</sup>N. N. Gorelenkov, E. Fredrickson, E. Belova, C. Z. Cheng, D. Gates, S. Kaye, and R. B. White, in 19th IAEA Fusion Energy Conference, Lyon, France, 14–19 October 2002 (IAEA, Vienna), paper IAEA-CN-94/TH/7-1 Ra.
- <sup>49</sup>N. N. Gorelenkov, C. Z. Cheng, G. Y. Fu, S. Kaye, R. White, and M. V. Gorelenkova, Phys. Plasmas **7**, 1433 (2000).
- <sup>50</sup>L. L. Lao, H. St. John, R. D. Stambaugh, A. G. Kellman, and W. P. Pfeiffer, Nucl. Fusion **25**, 1611 (1985).
- <sup>51</sup>S. A. Sabbagh, S. M. Kaye, J. E. Menard *et al.*, Nucl. Fusion **41**, 1601 (2001).
- <sup>52</sup>J. D. Strachan, B. Grek, W. Heidbrink, D. Johnson, S. M. Kaye, H. W. Kugel, B. LeBlanc, and K. McGuire, Nucl. Fusion **25**, 863 (1985).
- <sup>53</sup>D. S. Darrow, R. Bell, D. W. Johnson, H. Kugel, J. R. Wilson, R. E. Cecil, R. Maingi, A. Krasilnikov, and A. Alekseyev, Rev. Sci. Instrum. **72**, 784 (2001).
- <sup>54</sup>H. L. Berk, B. N. Breizman, J. Fitzpatrick, M. S. Pekker, H. V. Wong, and K. L. Wong, Phys. Plasmas **3**, 1827 (1996).
- <sup>55</sup>R. E. Bell, B. P. LeBlanc, C. Bourdelle *et al.*, Proceedings of 28th EPS Conference on Controlled Fusion and Plasma Physics, Funchal, 2001 (European Physical Society, Geneva, 2001), ECA Vol. 25A, p. 1021.
- <sup>56</sup>C. Z. Cheng, Phys. Rep. **211**, 1 (1992).
- <sup>57</sup>R. B. White and M. S. Chance, Phys. Fluids **27**, 2455 (1984).
- <sup>58</sup>D. Stutman, M. Finkenthal, V. Soukhanovskii, M. J. May, H. W. Moos, and R. Kaita, Rev. Sci. Instrum. **70**, 572 (1999).
- <sup>59</sup>S. Kaye, C. E. Bush, E. Fredrickson, B. LeBlanc, R. Maingi, and S. Sabbagh, "L-H mode transitions in the NSTX Spherical Torus: Experiment/theory comparisons," Phys. Plasmas (submitted).
- <sup>60</sup>S. S. Medley and A. L. Roquemore, Rev. Sci. Instrum. **69**, 2651 (1998).
- <sup>61</sup>S. S. Medley, R. E. Bell, M. P. Petrov, A. L. Roquemore, and E. V. Suvorkin, Rev. Sci. Instrum. **74**, 1892 (2003).
- <sup>62</sup>D. S. Darrow, S. J. Zweben, Z. Chang, C. Z. Cheng, M. D. Diesso, E. D. Fredrickson, E. Mazzucato, R. Nazikian, C. K. Phillips, S. Popovichev, M. H. Redi, R. B. White, J. R. Wilson, and K. L. Wong, Nucl. Fusion **37**, 939 (1997).